THE JOURNAL OF BIOLOGICAL CHEMISTRY VOL. 285, NO. 15, pp. 11584–11595, April 9, 2010

Terpestacin Inhibits Tumor Angiogenesis by Targeting UQCRB of Mitochondrial Complex III and Suppressing Hypoxia-induced Reactive Oxygen Species Production and Cellular Oxygen Sensing*[S]

Received for publication, November 24, 2009, and in revised form, January 25, 2010 Published, JBC Papers in Press, February 9, 2010, DOI 10.1074/jbc.M109.087809

Hye Jin Jung[‡1], Joong Sup Shim[‡1], Jiyong Lee[‡], Young Mi Song[‡], Ki Chung Park[§], Seung Hoon Choi[§], Nam Doo Kim[¶], Jeong Hyeok Yoon[¶], Paul T. Mungai[‖], Paul T. Schumacker[‖], and Ho Jeong Kwon[‡2]

From the [‡]Department of Biotechnology, Translational Research Center for Protein Function Control, College of Life Science and Biotechnology, Yonsei University, Seoul 120-749, Korea, the [§]Department of Surgery, College of Medicine, Yonsei University, Seoul 120-752, Korea, the [¶]Drug Design Team, Equispharm Inc., 864-1, Gyeonggi, Korea, and the [‖]Department of Pediatrics, Northwestern University, Chicago, Illinois 60611

Cellular oxygen sensing is required for hypoxia-inducible factor-1α stabilization, which is important for tumor cell survival, proliferation, and angiogenesis. Here we find that terpestacin, a small molecule previously identified in a screen of microbial extracts, binds to the 13.4-kDa subunit (UQCRB) of mitochondrial Complex III, resulting in inhibition of hypoxia-induced reactive oxygen species generation. Consequently, such inhibition blocks hypoxia-inducible factor activation and tumor angiogenesis *in vivo*, without inhibiting mitochondrial respiration. Overexpression of UQCRB or its suppression using RNA interference demonstrates that it plays a crucial role in the oxygen sensing mechanism that regulates responses to hypoxia. These findings provide a novel molecular basis of terpestacin targeting UQCRB of Complex III in selective suppression of tumor progression.

Progression of many solid tumors requires angiogenesis (1). Mitochondrial function has been linked to angiogenesis, because mitochondria are the primary sites of oxygen consumption, and angiogenesis is an oxygen concentration-sensitive process (2). Reports suggest that reactive oxygen species (ROS)[3] generation at mitochondrial Complex III is necessary and sufficient to trigger HIF-1α stabilization during hypoxia, and cells lacking mitochondrial DNA and electron transport activity (ρ^o cells) fail to exhibit increased ROS or up-regulation of HIF-1α target genes during hypoxia (3–5). Inhibitors of Complex III such as myxothiazol and stigmatellin also block mitochondrial ROS generation and inhibit the stabilization and transcriptional activity of HIF-1α during hypoxia. These findings suggest that the generation of ROS from mitochondrial Complex III is a critical event in the signaling of cellular hypoxia (6, 7). However, details regarding which of the components of Complex III contribute to this signaling remain to be described.

Biological screening tools are useful for identifying naturally occurring small molecules capable of inducing a specific phenotype change (8, 9). We performed a large scale screen of microbial extracts in an attempt to identify small molecules that could inhibit the angiogenic response to pro-angiogenic stimuli, such as hypoxia, in endothelial cells. We identified terpestacin as a small molecule with unique bicyclo sesterterpene structure capable of inhibiting the angiogenic response at concentrations below the toxic threshold (10). Terpestacin strongly inhibits the functional response to hypoxia of human umbilical vein endothelial cells *in vitro* and angiogenesis within the embryonic chick chorioallantoic membrane *in vivo*. In addition to this anti-angiogenic activity, terpestacin has previously been reported to inhibit syncytium formation during human immunodeficiency virus infection and has been chemically synthesized (11–13). However, neither the molecular target of this compound nor the cellular mechanism of its anti-angiogenic activity has been identified.

In the present study we identified the binding protein of terpestacin and clarified the cellular mechanism underlying its effects on angiogenesis. We find that terpestacin specifically binds to the 13.4-kDa subunit (UQCRB in human; accession number NM_006294; QCR7 in yeast; Sub 6 in bovine or chicken) of Complex III in the mitochondrial respiratory chain (14). The biological activity of terpestacin correlates significantly with the response to UQCRB knockdown in mammalian cells. The discovery that a small molecule targeting UQCRB in mitochondrial Complex III can prevent the angiogenic response *in vivo* and *in vitro* without inducing cell death implies

* This work was supported by the National R & D Program for Cancer Control, Ministry of Health & Welfare, the Translational Research Center for Protein Function Control, KRF Grant 2009-0083522, the National Research Foundation of Korea Grant funded by Korean Government Grant 2009-0092964, and the Brain Korea 21 project of the Republic of Korea. This work was supported, in whole or in part, by National Institutes of Health Grants HL35440 and HL079650 (to P. T. S. and P. T. M.).

[S] The on-line version of this article (available at http://www.jbc.org) contains supplemental Figs. S1–S5.

[1] Both authors contributed equally to this work.

[2] To whom correspondence should be addressed: Dept. of Biotechnology, College of Life Science and Biotechnology, Yonsei University, 134 Shinchon-dong, Seodaemun-gu, Seoul 120-749, Korea. Tel.: 82-2-2123-5883; Fax: 82-2-362-7265; E-mail: kwonhj@yonsei.ac.kr.

[3] The abbreviations used are: ROS, reactive oxygen species; VEGF, vascular endothelial growth factor; MG132, carboxybenzyl-leucyl-leucyl-leucinal; p70S6K, 70-kDa ribosomal protein S6 kinase; HIF, hypoxia-inducible factor; MR, magnetic resonance; SPR, surface plasmon resonance; ter-coumarin, coumarin-labeled terpestacin; siRNA, small interfering RNA; HUVEC, human umbilical vein endothelial cell; siUQCRB, siRNA specific for human UQCRB; SQ, semiquinone.

that UQCRB plays a key role in the cellular oxygen sensing and transduction system. This study provides new insight into the oxygen sensing role of UQCRB in mitochondrial Complex III, and a small molecule targeting that system provides a powerful tool for regulating tumor angiogenesis.

EXPERIMENTAL PROCEDURES

In Vivo Breast Cancer Xenograft Model Study—Twenty-four C3H/HeJ mice were inoculated subcutaneously with spontaneously occurring FM3A breast cancer cells. Twelve mice were treated intraperitoneally with terpestacin (2.5 μM) on days 0, 2, 4, 6, and 8. Another twelve mice were injected with saline as a negative control. On day 10, the tumor-bearing mice were examined with dynamic T1-weighted sequences using gadolinium diethylenetriaminepentaacetate in a 1.5T magnetic resonance (MR) scanner. After examination, the tumors were harvested for immunostaining of tumor blood vessels and expression of hypoxia-responsible genes, HIF-1α, and VEGF.

MRI—MRI was performed on a clinical 1.5 T whole body MR system (Gyroscan, Philips) using a custom-made radiofrequency coil for excitation and signal reception. All of the animals were examined with high resolution T1- and T2-weighted pulse sequences and dynamic contrast-enhanced T1-weighted MRI using the following imaging parameters: repetition time/echo time (T_R/T_E) = 500/10 ms, flip angle = 30°, acquisition = 8, matrix size = 256 × 198, slice thickness = 1.5 mm, and in-plane resolution = 234 × 234 μm.

Immunohistochemistry—Five-micrometer paraffin sections were incubated with anti-CD34 (Santa Cruz), anti-HIF-1α (Novus), and anti-VEGF (R & D Systems) mouse monoclonal antibodies for 1 h, respectively. After rinsing, the slides were incubated with secondary antibody for 45 min. The LSAB2/HRP staining kit (DakoCytomation) and the En Vision kit (DakoCytomation) were used for secondary antibody reaction. The slides were then washed and incubated with an avidin-biotin-peroxidase complex, followed by 3,3′-diaminobenzidine tetrahydrochloride color development. Counterstaining was performed using hematoxylin.

VEGF-Enzyme-linked Immunosorbent Assay—C3H mice with FM3A breast carcinomas were injected with either terpestacin or vehicle (saline) at 2-day intervals. The implants were harvested on day 7, and the concentration of VEGF protein in tumor tissue extracts was determined by a VEGF-enzyme-linked immunosorbent assay (R & D Systems) according to the manufacturer's instructions. VEGF protein levels were normalized to the total protein concentration of each sample.

Synthesis of Molecular Probes for Terpestacin—Biotinylated terpestacin with 1-ethyl-3-[3-dimethylaminopropyl] carbodiimide hydrochloride (1.5 mg, 0.0078 mmol) and dimethylaminopyridine (1.0 mg, 0.0082 mmol) were added to a stirred solution of terpestacin (3.0 mg, 0.0075 mmol) and *N*-(+)-biotinyl-6-aminohexanoic acid (2.7 mg, 0.0076 mmol; Pierce) in Me_2SO (3 ml) was added at 0 °C. After incubation overnight at room temperature, the crude product was extracted with EtOAc (15 ml) and purified by preparative TLC (CH_2Cl_2:methanol = 10:1) to yield two biotinylated terpestacin derivatives (hydroxyl group at the C-24 position (BT1) and hydroxyl group at the C-17 position (BT2)). This procedure resulted in 75% yield. The matrix-assisted laser desorption ionization-mass spectrometry value for $C_{41}H_{63}N_3O_7S$ was *m*/*z* 764.5 $[M + Na]^+$.

Coumarin-conjugated Terpestacin—1-Ethyl-3-[3-dimethylaminopropyl] carbodiimide hydrochloride (1.0 mg, 0.0052 mmol) and dimethylaminopyridine (0.64 mg, 0.0052 mmol) were added to a stirred solution of terpestacin (2.0 mg, 0.005 mmol) and Boc-6-aminohexanoic acid (1.2 mg, 0.0052 mmol) in dimethylformamide (2 ml) at 0 °C. After incubation overnight at room temperature, the crude product was extracted with EtOAc (4 ml × 3), treated with 20% trifluoroacetic acid in CH_2Cl_2 (1 ml), and stirred for 2 h at room temperature. *N*,*N*-diisopropylethylamine (1.3 mg, 0.01 mmol) and 6-((7-amino-4-methylcoumarin-3-acetyl) amino) hexanoic acid succinimidyl ester (2.2 mg, 0.005 mmol, Molecular Probes) were added at 0 °C. After stirring for 4 h at room temperature, the crude product was extracted with EtOAc (20 ml) and purified by preparative TLC (CH_2Cl_2:methanol = 10:1) to produce coumarin-conjugated terpestacin at 61% yield. Matrix-assisted laser desorption ionization-mass spectrometry for $C_{49}H_{71}N_3O_9$ *m*/*z* 868.5 $[M + Na]^+$.

Phage Display Affinity Selection—Biotinylated terpestacin was immobilized onto a streptavidin-coated plate (Pierce), and phage display was performed using T7 phages encoding human cDNA libraries from liver tumor, normal liver, Alzheimer's brain, normal brain, and normal stomach tissues (Novagen) as described previously (15). Specific terpestacin-binding phages were isolated and analyzed by DNA sequencing using the PRISM dye terminator cycle sequencing ready reaction kit (Applied Biosystems). The sequence homologies of the obtained sequences were compared with sequences in GenBank™ using the BLAST program.

Molecular Cloning, Expression, and Purification of Human UQCRB—For mammalian expression, the full-length human UQCRB expression vector was constructed by subcloning a PCR-amplified full-length cDNA of UQCRB (accession number NM_006294) into the EcoRI/XhoI site of pCDNA3.1-HA (Invitrogen). To obtain the recombinant UQCRB protein from bacteria, the UQCRB cDNA was inserted into the EcoRI/XhoI site of pGEX-4T1 (Amersham Biosciences). The glutathione *S*-transferase-UQCRB fusion protein was purified as described previously (16) and treated with thrombin (Amersham Biosciences) for the removal of glutathione *S*-transferase.

Site-directed Mutagenesis—The QuikChange site-directed mutagenesis system (Stratagene) was used to mutate selected codons in the clone of human UQCRB gene. The following primers were used: to change Leu^{32} to Ala, 5′-GCAGGATTCAATAAACTGGGGGCAATGCGAGATGATACA-3′ and 5′-TGTATCATCTCGCATTGCCCCCAGTTTATTGAATCCTGC-3′; and to change Ile^{63} to Ala, 5′-AATGACAGGATGTTTCGCGCTAAGAGGGCACTGGAC-3′ and 5′-GTCCAGTGCCCTCTTAGCGCGAAACATCCTGTCATT-3′. The mutated codons are underlined. PCR was performed under the following conditions: initial denaturation for 30 s at 95 °C, 16 cycles of 30 s at 95 °C, 1 min at 55 °C, and 12 min at 68 °C. After digestion of the parental DNA for 1 h at 37 °C with DpnI, the amplified plasmids were transformed into *Escherichia coli* XL-1 Blue competent cells. The presence of the mutation was confirmed by DNA sequencing.

Surface Plasmon Resonance (SPR) Analysis—Biotin and biotinylated terpestacin were sequentially immobilized on the surface of a streptavidin-coated sensor chip. Molecular interaction analysis was performed using the BIAcore 2000 (BIAcore AB) as described previously (15). The SPR response curves were analyzed with BIAcore Evaluations software, version 3.1. The apparent association and dissociation constants were calculated from the kinetic constants equations: $K_A = k_a/k_d$, $K_D = k_d/k_a$.

Docking Simulation—The structure of terpestacin was optimized employing the nonlocal density functional theory (B3LYP DFT) function and restricted Hartree-Fock (RHF)/6–31G(*) basis set description. All of the atomic charges were assigned using the Mullikan Populations of Gaussian 03 calculation result. To find out the docking structures of terpestacin into UQCRB, automated docking simulation was implemented with the program AutoDock version 3.0. The UQCRB structure was used for x-ray crystal structure from the Protein Data Bank (code 3BCC; chicken cytochrome bc_1 complex). An initial protein structure was energy minimized for 1000 steps employing the steepest descent algorithm. In AutoDock, docking was performed by combining a global genetic algorithm with local minimization, Lamarckian genetic algorithm. 100 trials of each docking were preformed, and final docked conformations were clustered using a tolerance of 1 Å root mean square deviation. The docking conformation properly oriented toward the UQCRB pocket was selected, and the free energy of binding was estimated.

Subcellular Localization Analysis of Terpestacin—For fluorescence microscope analysis, HT1080 cells were incubated with 20 μM of coumarin or coumarin-conjugated terpestacin (ter-coumarin) for 24 h in the presence or absence of excess terpestacin. After washing with phosphate-buffered saline, the cells were observed under a fluorescence microscope (Olympus). To determine the subcellular localization of terpestacin, HT1080 cells were grown on glass coverslips in 24-well plates and treated with 50 μM of coumarin or ter-coumarin for 30 min. To stain the mitochondria, the cells were treated with MitoTracker (100 nM, catalog number M-7512; Molecular Probes) at 37 °C for 15 min. After washing with phosphate-buffered saline, the cells were fixed with 4% formaldehyde, and the coverslips were mounted with a ProLong antifade kit (Molecular Probes) according to the manufacturer's instructions. The fluorescence image was obtained using a confocal laser scanning microscope (Axiovert 100M; Carl Zeiss).

Transcriptional Profiling—Total RNA was prepared from HT1080 cells using the TRIzol reagent (Invitrogen). The probe preparation and microarray hybridization was performed using the TwinChip Human-8K cDNA microarray (Digital Genomics) as described previously (17). Microarray data analysis was conducted using the GeneSight data analysis software (v3.5, BioDiscovery). Signature correlation coefficient values (ρ) between two experimental conditions were obtained as described previously (18).

Measurement of Mitochondrial Membrane Potential ($\Delta\Psi_m$)—The change in $\Delta\Psi_m$ was detected by a fluorescence-based assay. The cells were incubated for 4 h with radicicol or terpestacin and then stained for 15 min with 0.25 μg/ml of 5,5′,6,6′-tetrachloro-1,1′,3,3′-tetraethylbenzimidazol-carbocyanine iodide, which is a lipophilic cationic probe (JC-1; Molecular Probes). At hyperpolarized membrane potentials (to −140 mV), this dye forms a red fluorescent J-aggregate, whereas at depolarized membrane potentials (to −100 mV), this dye remains in its green fluorescent monomeric form. Subsequently, the cells were washed with phosphate-buffered saline twice. The images were obtained using an IX70 fluorescence microscope (Olympus) at a ×100 magnification.

Measurement of Mitochondrial Oxygen Consumption—Mitochondrial respiration was measured using succinate, a substrate for Complex II. When succinate (5 mM) was added to mitochondria, the flavin adenine dinucleotide-linked O_2 consumption was stimulated. Mouse liver mitochondria (0.2 mg/ml) were pretreated for 15 min with terpestacin (80 μg/ml), antimycin A (0.1 μg/ml), or methanol control (0.5%). The respiration rate of mitochondria was measured with Clark-type oxygen electrode (Oxygen electrode Units DW1; Hansatech Instruments) at 30 °C.

Cell Culture and Hypoxic Condition—Early passages (4–8 passages) of HUVECs were grown in endothelial cell medium-2 (EGM-2, Cambrex) supplemented with 10% fetal bovine serum (Invitrogen). HT1080 (fibrosarcoma) cells were maintained in minimum essential medium (Invitrogen) containing 10% fetal bovine serum. 143B (osteosarcoma), HepG2 (hepatoma), HeLa (cervical squamous carcinoma), CHANG (normal liver), and Hep3B (hepatoma) cells were grown in Dulbecco's modified Eagle's medium (Invitrogen) supplemented with 10% fetal bovine serum. All of the cells were maintained in a humidified 5% CO_2 incubator. For the hypoxic conditions, the cells were incubated at a CO_2 level of 5% with 1% O_2 balanced with N_2 in a hypoxic chamber (Forma).

Western Blot Analysis—The cell lysates were separated by 10% SDS-PAGE and were then transferred to polyvinylidene fluoride membranes (Milipore) using standard electroblotting procedures. The blots were then blocked and immunolabeled overnight at 4 °C with anti-HIF-1α (BD Biosciences), anti-VEGF (Santa Cruz), anti-phospho-p70S6K (Cell Signaling), anti-p70S6K (Cell Signaling), anti-β-actin, and anti-tubulin (Upstate Biotechnology Inc.) primary antibodies. Immunolabeling was detected by an ECL kit (Amersham Biosciences) according to the manufacturer's instructions.

Measurement of ROS—Intracellular ROS levels were measured using 2′,7′-dichlorofluorescein diacetate (Sigma). ROS in the cells cause oxidation of 2′,7′-dichlorofluorescein, generating a fluorescent product, 2′,7′-dichlorofluorescein. After incubation with 2′,7′-dichlorofluorescein diacetate (10 μM) for 10 min, the cells were lysed and centrifuged to remove debris. The fluorescence in the protein-normalized supernatant was determined using a FL600 microplate fluorescence reader (Bio-Tek) at the excitation and emission wavelengths of 485 and 535 nm, respectively.

Overexpression and RNA Interference Studies of UQCRB—For UQCRB overexpression, HT1080 cells were transfected with either control (neo) or UQCRB expression vectors (1 μg) using the SuperFect® transfection reagent (Qiagen). Human UQCRB-specific siRNA was constructed using the Stealth™ RNA interference (Invitrogen). For the knockdown of UQCRB

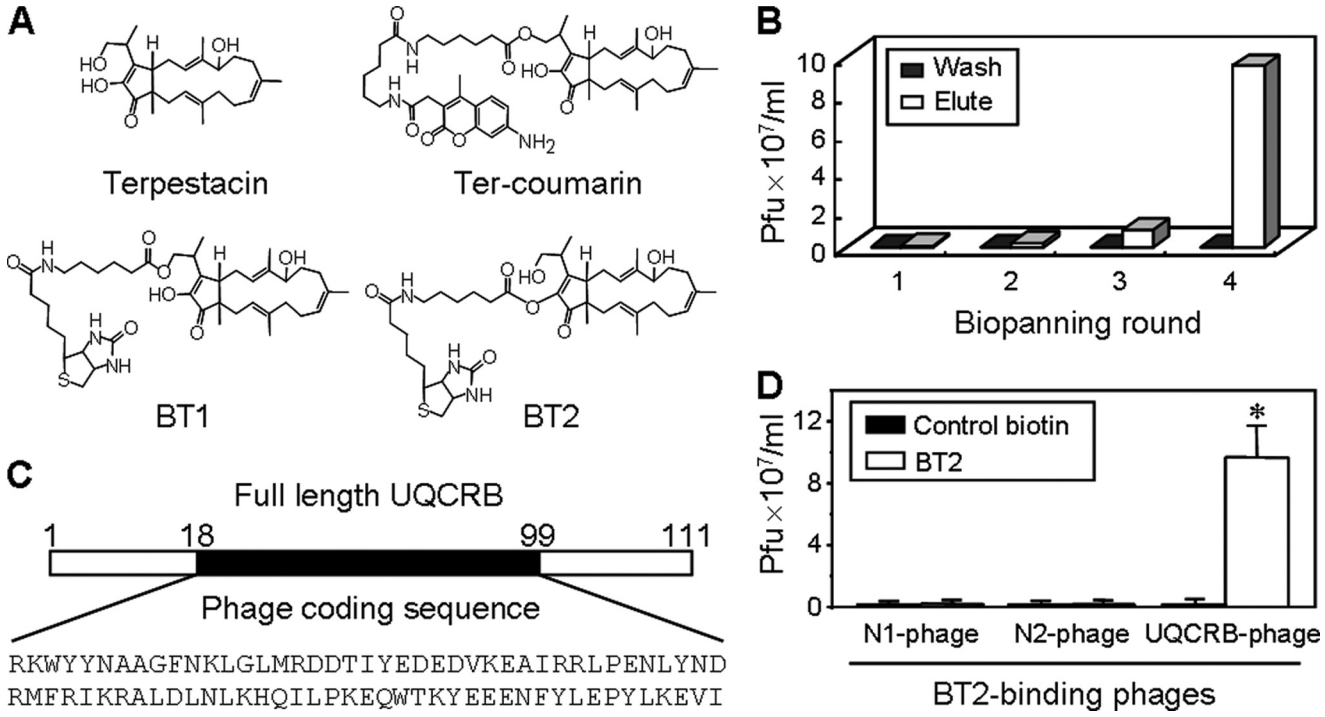

FIGURE 1. **Identification of terpestacin-binding protein using phage display affinity selection.** *A*, the structures of terpestacin and the molecular probes, including coumarin-conjugated terpestacin (*ter-coumarin*) and the biotinylated terpestacin derivatives (*BT1* for C-24 position and *BT2* for C-17 position of hydroxyl groups). *B*, analysis of the number of terpestacin-binding phages eluted after each round of biopanning (*Elute*). *Wash* indicates nonspecific phages bound to biotinylated terpestacin immobilized onto streptavidin-coated wells. *Pfu*, phage plaque-forming unit. *C*, coding region of terpestacin-binding phages of human full-length UQCRB. *D*, the specificity of the interaction between BT2 and UQCRB-expressing phages. Control biotin and nonspecific phages (*N1* and *N2*) were used as negative controls for BT2 and UQCRB phage, respectively. *, $p < 0.001$ *versus* control biotin. Each value represents the mean ± S.E. from three independent experiments.

mRNA, HT1080 cells were transfected with either control or UQCRB siRNA (5, 10 nM) using the Lipofectamine™ 2000 transfection reagent (Invitrogen) according to the manufacturer's instructions. Interference of UQCRB mRNA was validated though reverse transcription-PCR analysis using specific primers for UQCRB.

In Vitro Invasion and Angiogenesis Assays—The invasiveness of endothelial or tumor cells was examined using a Transwell chamber system with 8.0-μm pore-sized polycarbonate filter inserts (Corning Costar). The total number of invaded cells was counted using an optical microscope at a ×100 magnification. The tube formation assay was conducted using HUVECs grown on Matrigel as described previously (10). Tube formation was quantified by counting the number of connected cells in randomly selected fields at a ×100 magnification and dividing that number by the total number of cells in the same field.

Materials—Terpestacin was purified from the culture extract of a fungal strain, *Embellisia chlamydospora*, as described previously (10). Antimycin A, myxothiazol, and rotenone were purchased from Sigma, and stigmatellin was purchased from Fluka.

Statistical Analysis—The results are expressed as the means ± S.E. The Student's *t* test was used to determine statistical significance between control and test groups. A *p* value of <0.05 was considered statistically significant.

RESULTS

Identification of Human UQCRB as a Terpestacin-binding Protein—To explore the molecular mechanisms underlying inhibition of angiogenesis by terpestacin, phage display biopanning, an approach that has proven to be a powerful means to identify cellular binding proteins of bioactive small molecules, was applied to identify terpestacin binding proteins (15, 19). Terpestacin was biotinylated at either the C-24 (BT1) or C-17 (BT2) position hydroxyl group to produce an affinity ligand for the isolation of its binding proteins (Fig. 1*A*). Both BT1 and BT2 retained their biological activity, as shown by their anti-proliferative activities in HUVECs. BT1 was first immobilized on a streptavidin-coated well plate, and four rounds of phage biopanning were conducted using T7 phages expressing functional human cDNA libraries (6×10^9 phage plaque-forming unit/ml). After the fourth round of biopanning, phage particles that bound specifically to BT1 were isolated and analyzed by DNA sequencing (Fig. 1*B*). Among a total of 18 phage plaques isolated for DNA sequencing, all phage clones (100%) were identified as human UQCRB-encoding phages (Fig. 1*C*). An independent experiment was performed using BT2 affinity ligand using the same procedure as for BT1. As the result, more than 90% (18 of a total of 20 phage clones) of BT2-binding phages were expressing UQCRB. The remaining BT2-binding phage clones were found to represent nonspecific binders (Fig. 1*D*). The highly enriched biopanning result of phage display with two biotinylated terpestacins strongly demonstrate that UQCRB is the highest affinity binding protein of terpestacin.

Analysis of the Molecular Interaction between Terpestacin and UQCRB—To verify the specific binding of terpestacin to UQCRB, a phage display binding assay was investigated first with diverse classes of biologically active small molecules. The

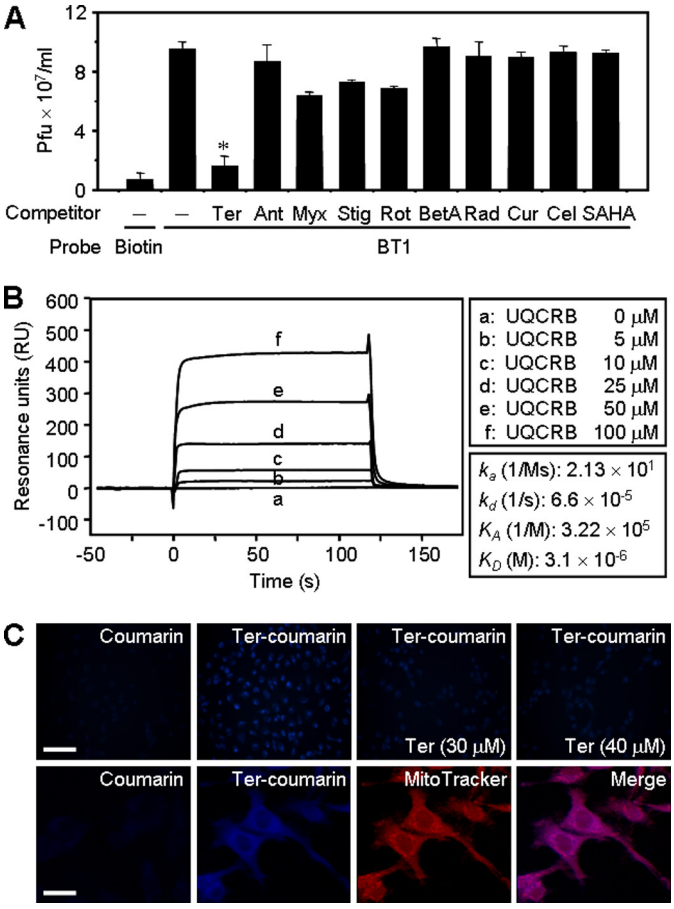

FIGURE 2. **Molecular interactions and subcellular localization of terpestacin.** *A*, effects of various competitors on the binding between UQCRB phages and immobilized terpestacin. All of the competitors were used at a concentration of 100 μM. *Ter*, terpestacin; *Ant*, antimycin A; *Myx*, myxothiazol; *Stig*, stigmatellin; *Rot*, rotenone; *BetA*, betulinic acid; *Rad*, radicicol; *Cur*, curcumin; *Cel*, celecoxib; *SAHA*, suberoylanilide hydroxamic acid; *Pfu*, phage plaque-forming unit. *, $p < 0.001$ *versus* no competitor control. Each value represents the mean ± S.E. from three independent experiments. *B*, SPR analysis of the interaction between terpestacin and purified recombinant UQCRB at various concentrations. The results shown are representative of three independent experiments. *C*, binding of ter-coumarin (20 μM) to a specific target in cells in the presence of excess terpestacin (30 or 40 μM) through a fluorescence microscope (*upper panels*). Scale bar, 200 μm. Colocalization of ter-coumarin (*blue*) and MitoTracker (*red*) using a confocal microscope (*lower panels*). *Scale bar*, 20 μm. The results shown are representative of three independent experiments.

binding of UQCRB-encoding phages to BT1 was completely abolished in the presence of excess free terpestacin but was not influenced by other mitochondrial inhibitors or by other angiogenesis inhibitors (Fig. 2*A*), implying that terpestacin specifically binds to UQCRB and is the first small molecule targeting UQCRB.

Next, the interaction between terpestacin and intact human UQCRB was demonstrated by surface plasmon resonance (BIAcore) analysis. The apparent binding affinities were calculated by subtraction of resonance values of UQCRB binding to control biotin from those of UQCRB binding to BT1. This analysis yielded specific binding curves for UQCRB to BT1 from the BIAcore sensorgrams, and the apparent dissociation constant (K_D) of UQCRB binding to terpestacin was calculated as 3.1×10^{-6} M (Fig. 2*B*). These results clearly demonstrate that UQCRB is a direct binding protein of terpestacin at micromolar levels close to its effective concentration toward the anti-angiogenic activity (5–10 μM).

Next, the interaction between terpestacin and UQCRB in the cellular level was assessed on the basis of the subcellular localization of ter-coumarin as a probe. Indeed, ter-coumarin intensively stains the cytoplasmic part of HT1080 fibrosarcoma cells, whereas control coumarin does not (Fig. 2*C*, *upper panels*). Pretreatment with excess free terpestacin in the cells dose-dependently decreased the fluorescence intensity of ter-coumarin, demonstrating that the probe specifically binds to the terpestacin target proteins in the cells. Furthermore, confocal microscopy analysis using ter-coumarin and a mitochondrial specific marker, MitoTracker, revealed the fluorescence signal of ter-coumarin coincided exactly with that of MitoTracker (Fig. 2*C*, *lower panels*), implying again that terpestacin binds to mitochondria in the cells where its target, UQCRB, is located.

To further elucidate the binding mode of terpestacin to UQCRB at molecular level, we simulated a binding model of UQCRB with terpestacin using the reference protein (Protein Data Bank code 3BCC; chicken cytochrome bc_1 complex) (20) and the AutoDock program. The docking modeling revealed that terpestacin binds to the hydrophobic pocket of UQCRB via its large hydrophobic ring structure, and nonpolar amino acid residues, including Leu^{32} and Ile^{63} of UQCRB, appear to be crucial for the hydrophobic interaction (Fig. 3, *A* and *B*). In addition, this model showed that terpestacin binds to the interface of the binding site between UQCRB and cytochrome *b*, suggesting that terpestacin could affect the interaction between cytochrome *b* and UQCRB. To verify this binding model of terpestacin and UQCRB, we constructed UQCRB mutants including L32A, I63A, and L32A/I63A and examined the binding affinity of these mutants to terpestacin by SPR analysis. The binding efficiency of L32A and I63A to terpestacin was decreased to 65 and 25%, respectively (Fig. 3*C*). Notably, the combined mutant of L32A and I63A completely abolished the binding with terpestacin. Bovine serum albumin as a negative control did not bind to terpestacin. These results validate the binding model that represents the significance of hydrophobic amino acid residues of UQCRB for the binding to terpestacin.

In addition, the functional genomic consequences of terpestacin binding to UQCRB was investigated by using cDNA microarray analysis of transcriptional changes in HT1080 cells treated with terpestacin or siRNA directed against human UQCRB (siUQCRB). The genome-wide gene expression profiling showed a significant correlation between terpestacin and UQCRB genetic knockdown, validating that UQCRB is a biologically relevant target of terpestacin (supplemental Fig. S1). All of these *in vitro* and *in vivo* data strongly demonstrate that UQCRB of mitochondrial Complex III is a cellular target protein of terpestacin and suggest a critical role for UQCRB in angiogenesis.

Terpestacin Decreases the Mitochondrial Membrane Potential ($\Delta\Psi_m$) without Inhibiting Mitochondrial Respiration—Next, we investigated the biological implication of the binding of terpestacin to UQCRB. To elucidate whether this interaction causes mitochondrial dysfunction, the mitochondrial membrane potential ($\Delta\Psi_m$) was measured using the JC-1 fluorescent marker. As shown in Fig. 4*A*, control HT1080 cells or cells

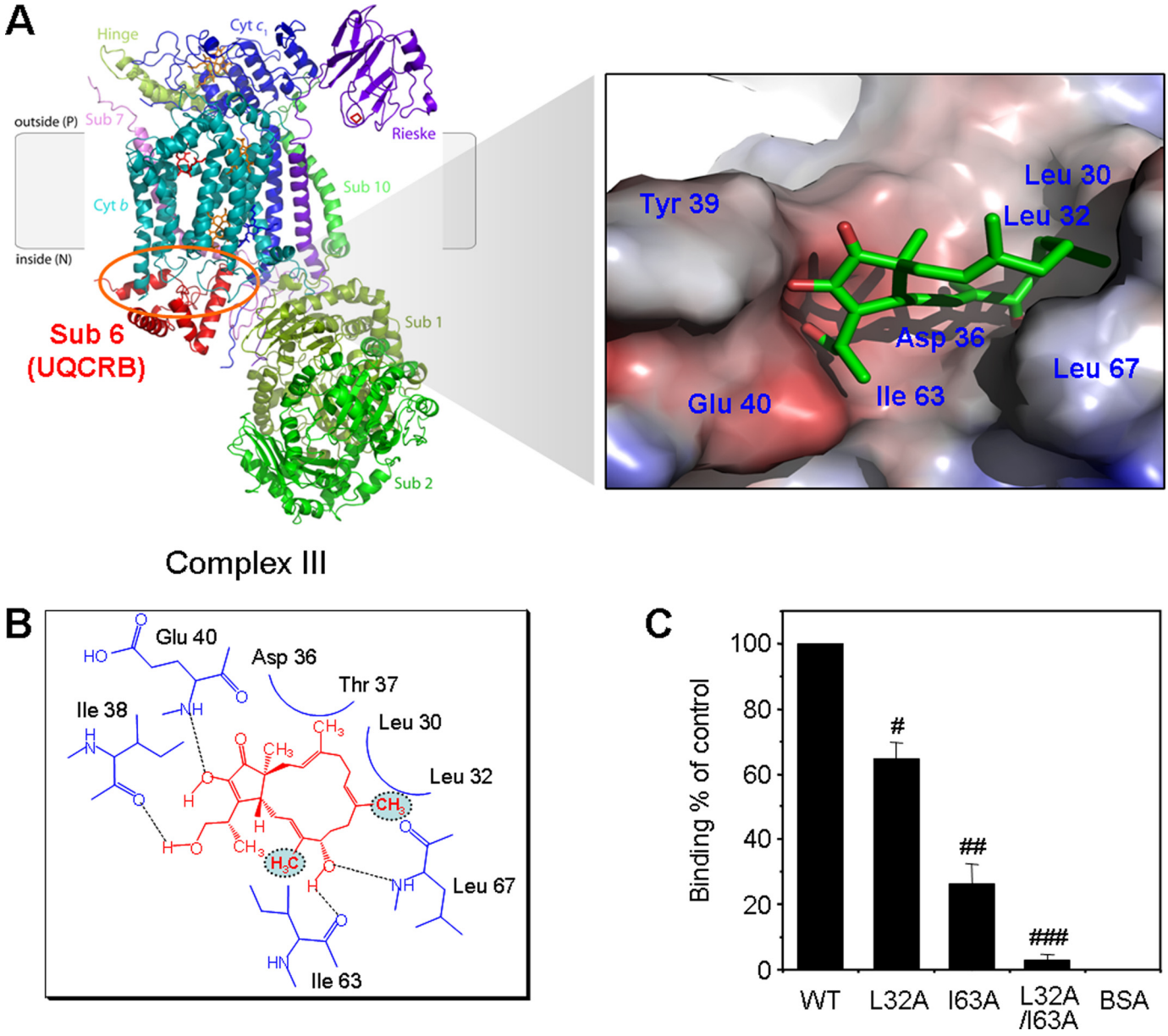

FIGURE 3. **Docking model of terpestacin-UQCRB complex.** *A*, electrostatic surface representation of the hydrophobic pocket of UQCRB bound with terpestacin. The *red* color denotes electronegative charge potential, and the *blue* color denotes electropositive charge potential. *B*, docking model analysis of terpestacin (*red*) and UQCRB (*blue*). The *dotted circles* indicate hydrophobic interaction of the complex. *C*, SPR analysis of the interaction between terpestacin and UQCRB wild and mutants. The binding efficiency of wild type (*WT*) UQCRB to terpestacin was defined as 100%. #, $p < 0.03$; ##, $p < 0.01$; ###, $p < 0.007$ *versus* *WT* UQCRB. Each value represents the mean ± S.E. from three independent experiments.

treated with radicicol, a structurally related molecule targeting heat shock protein 90 (Hsp90), exhibited a low level of green fluorescence and a high red-orange fluorescence (large negative $\Delta\Psi_m$). However, treatment with terpestacin led to an increase in green fluorescence and a decrease in red-orange fluorescence in a dose-dependent manner (loss of $\Delta\Psi_m$). These data demonstrate that the binding of terpestacin to UQCRB results in a mitochondrial response involving a dissipation of the mitochondrial membrane potential.

To further examine whether the binding of terpestacin to UQCRB affects mitochondrial energy metabolism, the mitochondrial oxygen consumption was measured using mouse liver mitochondria and succinate, a substrate for Complex II. As shown in Fig. 4*B*, mitochondrial respiration was strongly inhibited by antimycin A, whereas terpestacin did not inhibit oxygen consumption generated by the oxidation of succinate, implying that terpestacin regulates the function of mitochondrial Complex III without disrupting respiration, making it likely that ATP generation is not affected.

Terpestacin Suppresses Mitochondrial ROS Generation and HIF-1α Stabilization under Hypoxic Conditions—Mitochondrial Complex III is a major site of cellular ROS generation during hypoxia and is known to be involved in cellular oxygen sensing (5). Moreover, the increase in ROS production during hypoxia has been reported to initiate the stabilization of HIF-1α protein and to mediate hypoxia-induced transcription of genes such as VEGF (4). To examine whether terpestacin affects Complex III-derived ROS generation during hypoxia,

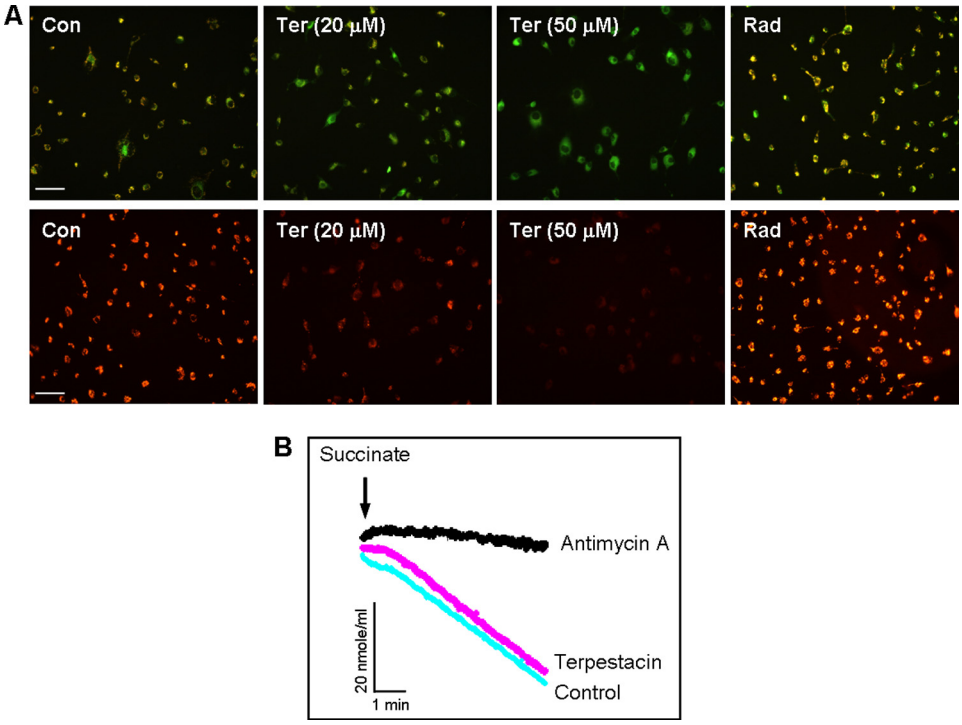

FIGURE 4. **Effects of terpestacin on mitochondrial membrane potential ($\Delta\Psi_m$) and mitochondrial respiration.** *A*, HT1080 cells were incubated for 4 h with terpestacin (*Ter*, 20 or 50 μM) or radicicol (*Rad*, 10 μM) and then stained with 0.25 μg/ml of JC-1 for 15 min. Fluorescence images were obtained with a fluorescence microscope. *Scale bar*, 200 μm. The results shown are representative of three independent experiments. *B*, mouse liver mitochondria (0.2 mg/ml) were pretreated for 15 min with terpestacin (80 μg/ml), antimycin A (0.1 μg/ml), or methanol control (*Con*, 0.5%). The respiration rate of mitochondria was measured with Clark-type oxygen electrode at 30 °C. The results shown are representative of two independent experiments.

we assessed intracellular ROS levels in HT1080 cells using the oxidant-sensitive fluorescent probe, 2′,7′-dichlorofluorescein. Terpestacin significantly suppressed the hypoxia-induced ROS generation in HT1080 cells (Fig. 5*A*). However, antimycin A, an inhibitor of downstream end of Complex III, did not elicit a decrease in ROS generation during hypoxia.

HIF-1α stabilization represents a functional response to hypoxia triggered by the cellular oxygen sensing system. We investigated the effect of terpestacin on HIF-1α stabilization to assess its influence on the cellular response to hypoxia. Hypoxia-induced accumulation of HIF-1α protein was dose-dependently inhibited by terpestacin (Fig. 5*B*). The HIF-1α destabilizing activity of terpestacin during hypoxia was verified in a number of animal cell lines as well (supplemental Fig. S2). To clarify that terpestacin affects HIF-1α stability induced by hypoxia, we next performed time course experiments of HIF-1α accumulation in the presence of terpestacin before or after hypoxia. As shown in Fig. 5*C*, terpestacin treatment before as well as after hypoxia expose effectively inhibited HIF-1α accumulation, implying that the HIF-1α destabilizing activity of terpestacin results from the suppression of ROS generation induced by hypoxia. To further verify whether terpestacin inhibits the stabilization of HIF-1α via suppression of Complex III-derived ROS generation, the effect of terpestacin on desferrioxamine-induced accumulation of HIF-1α protein was investigated. Previous reports revealed that the iron chelator desferrioxamine induces HIF-1α stabilization but does not require mitochondrial ROS (4). Terpestacin markedly inhibited the stabilization of HIF-1α during hypoxia but not during desferrioxamine treatment (Fig. 5*D*), demonstrating that terpestacin inhibits the stabilization of HIF-1α by suppressing mitochondrial ROS.

Next, we examined whether terpestacin-mediated inhibition of HIF-1α accumulation is associated with altered HIF-1α protein synthesis. MG132, a specific proteasome inhibitor, was used to block ubiquitin-dependent HIF-1α degradation. As expected, treatment with MG132 resulted in a marked accumulation of ubiquitinated HIF-1α proteins during hypoxia (Fig. 5*E*). By contrast, the inhibition of protein synthesis with cycloheximide blocked the accumulation of HIF-1α induced by hypoxia. Treatment with terpestacin under hypoxia in the presence of MG132 led to a substantial reduction of ubiquitinylated HIF-1α protein, suggesting that terpestacin may affect the upstream step of HIF-1α protein degradation by ubiquitin-proteasome pathway. In addition, the compound inhibited the phosphorylation of p70S6K, a downstream effector of phosphoinositide 3-kinase/Akt/mammalian target of rapamycin pathway that is implicated in the regulation of HIF-1α expression at the translational level (Fig. 5*F*) (21, 22). However, terpestacin did not affect mRNA level of HIF-1α, suggesting that the reduction of HIF-1α protein level by terpestacin is not due to the transcriptional reduction of HIF-1α gene (Fig. 5*G*). Moreover, terpestacin alone exhibited a much higher reduction of HIF-1α protein than that of MG132 in combination under hypoxic conditions, suggesting that terpestacin may inhibit both protein synthesis and stability of HIF-1α through suppression of Complex III-derived ROS generation during hypoxia.

Terpestacin Inhibits Hypoxia-induced Tumor Angiogenesis in an Animal Model System—HIF-1α plays a crucial role in tumor angiogenesis through the up-regulation of its angiogenic transcription products. We thus investigated the effect of terpestacin on tumor angiogenesis in a murine breast carcinoma xenograft model. C3H/HeJ mice were inoculated with spontaneously occurring FM3A breast cancer cells, and the mice were treated with or without terpestacin intraperitoneally. The tumor-bearing mice were examined with dynamic T1-weighted sequences using gadolinium diethylenetriaminepentaacetate in a 1.5T MR scanner. The MR amplitude, which reflects plasma volume, and the Kep parameter, which is influenced by the vessel permeability, were calculated using a two-compartment model. The resulting MR signal intensity was ~3-fold weaker in mice treated with terpestacin than in the saline control at the 900-s time point (Fig. 6*A*), indicating that

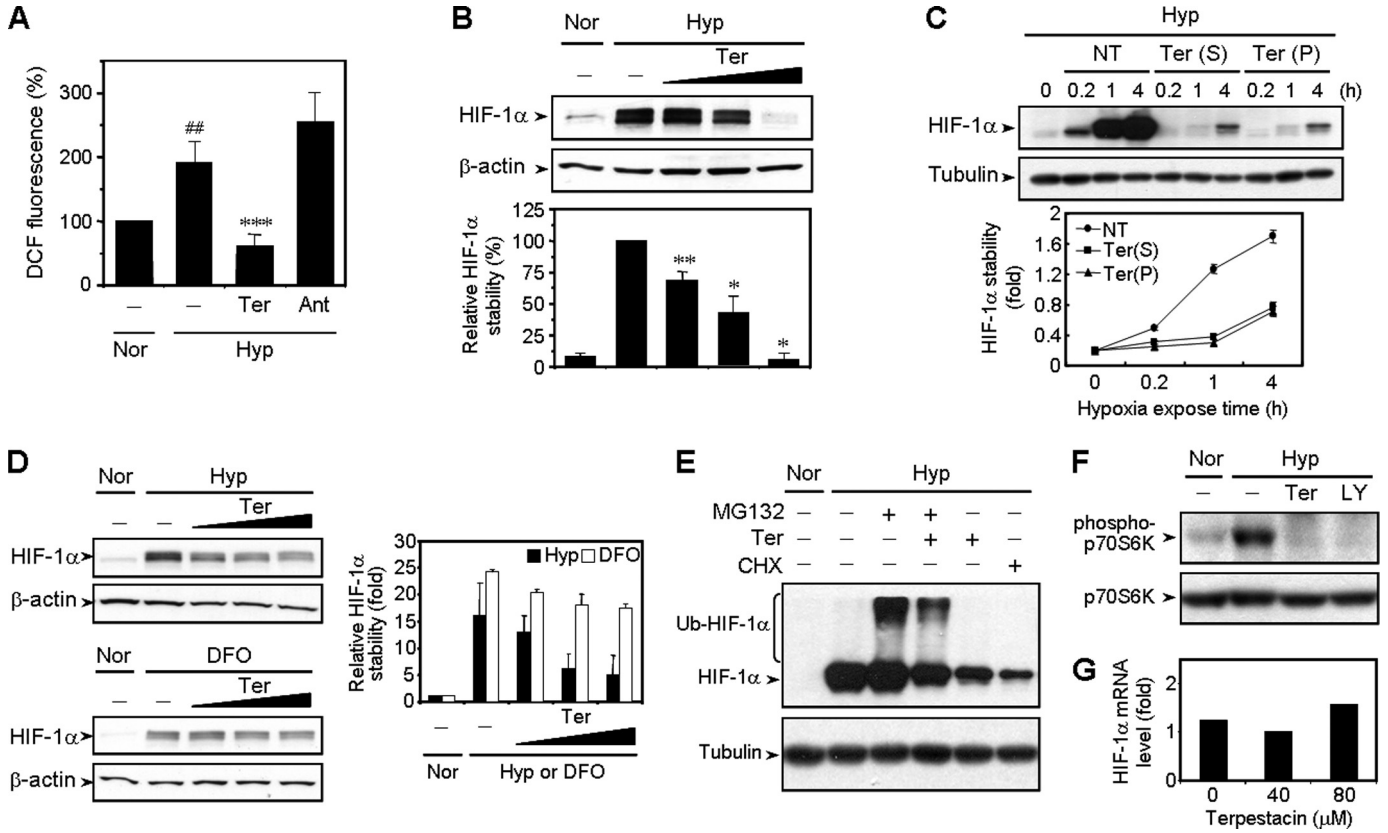

FIGURE 5. **Effects of terpestacin on mitochondrial ROS generation and HIF-1α stability.** *A*, intracellular ROS levels were determined by the 2′,7′-dichlorofluorescein (*DCF*) fluorescence. HT1080 cells were pretreated with terpestacin (*Ter*, 30 μM) or antimycin A (10 μM) for 30 min and then exposed to 1% $O_2$for 2 h. *Nor*, normoxia; *Hyp*, hypoxia. ##, $p < 0.01$ *versus* normoxic control; ***, $p < 0.005$ *versus* hypoxic control. Each value represents the mean ± S.E. from three independent experiments. *B*, HIF-1α protein levels were analyzed using Western blot analysis. The cells were pretreated with terpestacin for 30 min and then exposed to 1% O_2 for 4 h (*upper panel*). Western blot data were quantitated using densitometry (*lower panel*). **, $p < 0.002$; *, $p < 0.001$ *versus* hypoxic control. Each value represents the mean ± S.E. from three independent experiments. *C*, HIF-1α protein levels in cells exposed to 1% O_2 for the indicated times in the absence (*NT*, not treated with terpestacin) or presence of terpestacin (50 μM, before (*P*) or after (*S*) hypoxia expose). The cells were pretreated with terpestacin for 30 min and then exposed to 1% O_2(*P*). The cells were exposed to 1% O_2 and simultaneously treated with terpestacin (*S*). The results shown are representative of three independent experiments. *D*, HIF-1α protein levels in cells exposed to 1% O_2 or desferrioxamine (*DFO*, 100 μM) for 4 h with or without terpestacin. The level of β-actin was used as an internal control for normalization. The results shown are representative of three independent experiments. *E*, cells were incubated for 2 h under hypoxic conditions. The cells were then treated for additional 1 h under the same atmospheres in the presence of MG132 (20 μM), cycloheximide (*CHX*, 100 μM), or terpestacin (50 μM). The results shown are representative of two independent experiments. *F*, effect of terpestacin on the phosphorylation of p70S6K. The cells were incubated for 30 min in hypoxia in the presence of terpestacin (50 μM) or LY294002 (*LY*, 20 μM). The results shown are representative of three independent experiments. *G*, cells were pretreated with terpestacin (40 and 80 μM) for 30 min and then exposed to 1% O_2 for 4 h. HIF-1α mRNA levels were determined by quantitative PCR.

terpestacin efficiently inhibits the formation of blood vessels within the tumor.

After examination, the tumors were harvested for immunostaining of tumor blood vessel density using an anti-CD34 antibody. High blood vessel density was observed in control tumor tissues, whereas a significant decrease in the vessel density was observed in the animals treated with terpestacin (Fig. 6*B*). These data demonstrate that terpestacin effectively inhibits tumor angiogenesis *in vivo*.

VEGF is a major target gene of HIF-1α and plays a critical role in hypoxia-induced angiogenesis. We therefore examined the effect of terpestacin on HIF-1α and VEGF expression in the murine breast carcinoma xenograft model by immunohistochemical staining. In saline control tumors, many blood vessels were found, and HIF-1α and VEGF were highly expressed (Fig. 6*C*). However, HIF-1α and VEGF expression as well as blood vessel formation were markedly reduced in terpestacin-treated tumors. Moreover, compared with controls, terpestacin significantly decreased VEGF protein levels in the mouse tumor tissue extracts (Fig. 6*D*). These data indicate that terpestacin inhibits hypoxia-induced tumor angiogenesis via the inhibition of HIF-1α-mediated VEGF expression.

Implication of UQCRB in Hypoxia-induced Angiogenesis—As inferred from the results of the biological activity of terpestacin, UQCRB may play an important role in modulating the ROS- and HIF-mediated angiogenesis during hypoxia. To elucidate the role of UQCRB in angiogenesis, we conducted both UQCRB overexpression and knockdown experiments in HT1080 cells, and the resulting phenotypes were analyzed. First, HT1080 cells were transiently transfected with a vector containing the full-length UQCRB gene or control and examined for their invasive potential under normoxic conditions. Overexpression of UQCRB in HT1080 cells significantly increased the invasion of the tumor cells under normoxia (Fig. 7*A*). To examine the involvement of ROS in the promotion of tumor cell invasion by UQCRB, the intracellular ROS level was measured using 2′,7′-dichlorofluorescein fluorescence analysis. Increased 2′,7′-dichlorofluorescein fluorescence was

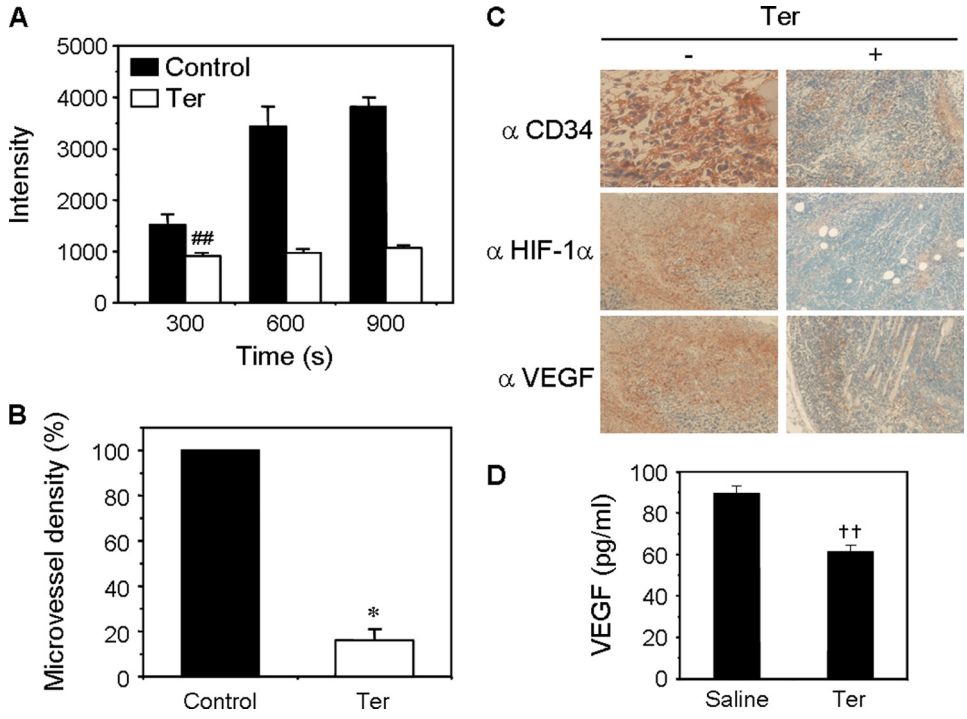

FIGURE 6. **Effect of terpestacin on tumor angiogenesis *in vivo*.** Mice bearing FM3A breast tumors were treated with saline (*control*) or terpestacin (*Ter*, one-third of LD_{50}, LD_{50} = 7.5 μM). *A*, time course of dynamic contrast-enhanced magnetic resonance signal intensity change associated with neovasculature. ##, $p < 0.01$ *versus* saline control. *B*, immunohistochemistry of tumor vasculature in paraffin sections of tumor tissues was performed using an antibody against the vascular antigen CD34. The microvessel density of control tumor tissues was defined as 100%. *, $p < 0.001$ *versus* saline control. *C*, effect of terpestacin on expression of hypoxia-responsible genes in murine tumor angiogenesis model. Tumor sections treated with saline (*left panels*) or terpestacin (*right panels*) were immunostained by antibodies against CD34 (*top panels*), HIF-1α (*middle panels*), and VEGF (*bottom panels*), respectively. *D*, effect of terpestacin on VEGF expression in mouse xenografts. The concentration of VEGF protein in tumor tissue extracts was determined by a VEGF-enzyme-linked immunosorbent assay. ††, $p < 0.05$ *versus* saline control.

observed in UQCRB transfected cells under normoxia (Fig. 7*B*). Notably, terpestacin, but not antimycin A, dose-dependently inhibited the UQCRB-induced ROS generation in HT1080 cells. Moreover, overexpression of UQCRB slightly, but reproducibly, increased the protein stability of HIF-1α under normoxia (Fig. 7*C*). An increase in the HIF-1α stability during UQCRB overexpression was comparable with that induced by cobalt chloride treatment, which has been shown to mimic the transcriptional response to hypoxia by inhibiting HIF-1α degradation. Expression of VEGF was also increased by UQCRB overexpression in HT1080 cells under normoxia (Fig. 7*D*). However, expression of VEGF receptors, such as Flt-1 and KDR, was not significantly changed by UQCRB overexpression.

Second, we investigated the effect of siUQCRB on the angiogenesis promoting potential of HT1080 cells under hypoxia. HT1080 cells were transfected with either siUQCRB or control siRNA and incubated in a hypoxic chamber. Knockdown of UQCRB gene by siUQCRB was confirmed through reverse transcription-PCR analysis (Fig. 7*E*). We first investigated the effect of UQCRB knockdown on the HIF-1α protein stability and VEGF expression in HT1080 cells. Hypoxia strongly increased both the protein stability of HIF-1α and the level of VEGF in HT1080 cells (Fig. 7*F*). These hypoxic effects were significantly blocked by UQCRB knockdown. Next, the conditioned media from the HT1080 cells incubated in each culture condition were collected and subjected to *in vitro* angiogenesis assays. The conditioned media from HT1080 cells incubated in the hypoxic chamber strongly activated the invasion and tube formation of HUVECs (Fig. 7*G*). However, the conditioned media from siUQCRB transfected HT1080 cells completely blocked the hypoxia-induced tumor angiogenesis of HUVECs. These data strongly demonstrate that UQCRB in mitochondrial Complex III is a critical mediator of hypoxia-induced tumor angiogenesis via ROS-mediated signaling originating from a mitochondrial O_2 sensor.

DISCUSSION

The present study reveals a novel role of UQCRB of the mitochondrial Complex III as a component of an oxygen sensor, through the identification of the protein target and the mode of action of a unique small molecule probe, terpestacin. Target validation was conducted using a number of biophysical, cell biological, and genome-wide transcriptional profiling of cells treated with the drug or subjected to genetic knockdown. Collectively, the data report for the first time on the role of UQCRB as a key component in the mitochondrial Complex III as an oxygen sensor and the mode of action of terpestacin at the molecular level (Fig. 7*H*).

Terpestacin Modulates the O_2-Sensing Function of Complex III by Targeting UQCRB without Acting as a Respiratory Poison—Utilizing the Q-cycle, Complex III (cytochrome bc_1 complex) transfers electrons from ubiquinol to cytochrome *c* and contributes to the generation of an electrochemical proton gradient (23–25). Two electrons from the oxidation of ubiquinol are conveyed to the high and low potential redox chains comprising the Rieske iron-sulfur cluster and c_1 heme and the b_L and b_H hemes, respectively (23). After the first electron is transferred to the Rieske iron-sulfur cluster, a semiquinone (SQ) radical intermediate in the Q_o site of cytochrome *b* (intermembrane space side of the mitochondrial inner membrane) donates the second electron to the low potential chain. Such efficient splitting of electrons between the high and low potential chains allows complex III to serve a role in energy transduction without deleterious side reactions, but when the bifurcation reaction is partially blocked, the SQ intermediate is likely to give an electron to O_2, resulting in the formation of superoxide (26, 27). Intriguingly, although the generation of ROS by any mechanism is an O_2-dependent process, an increase in mitochondrial ROS at lower O_2 levels (1–5% O_2) in intact cells suggests that during hypoxia, the lifetime of SQ may be prolonged, thereby promoting ROS generation (26), which is released into

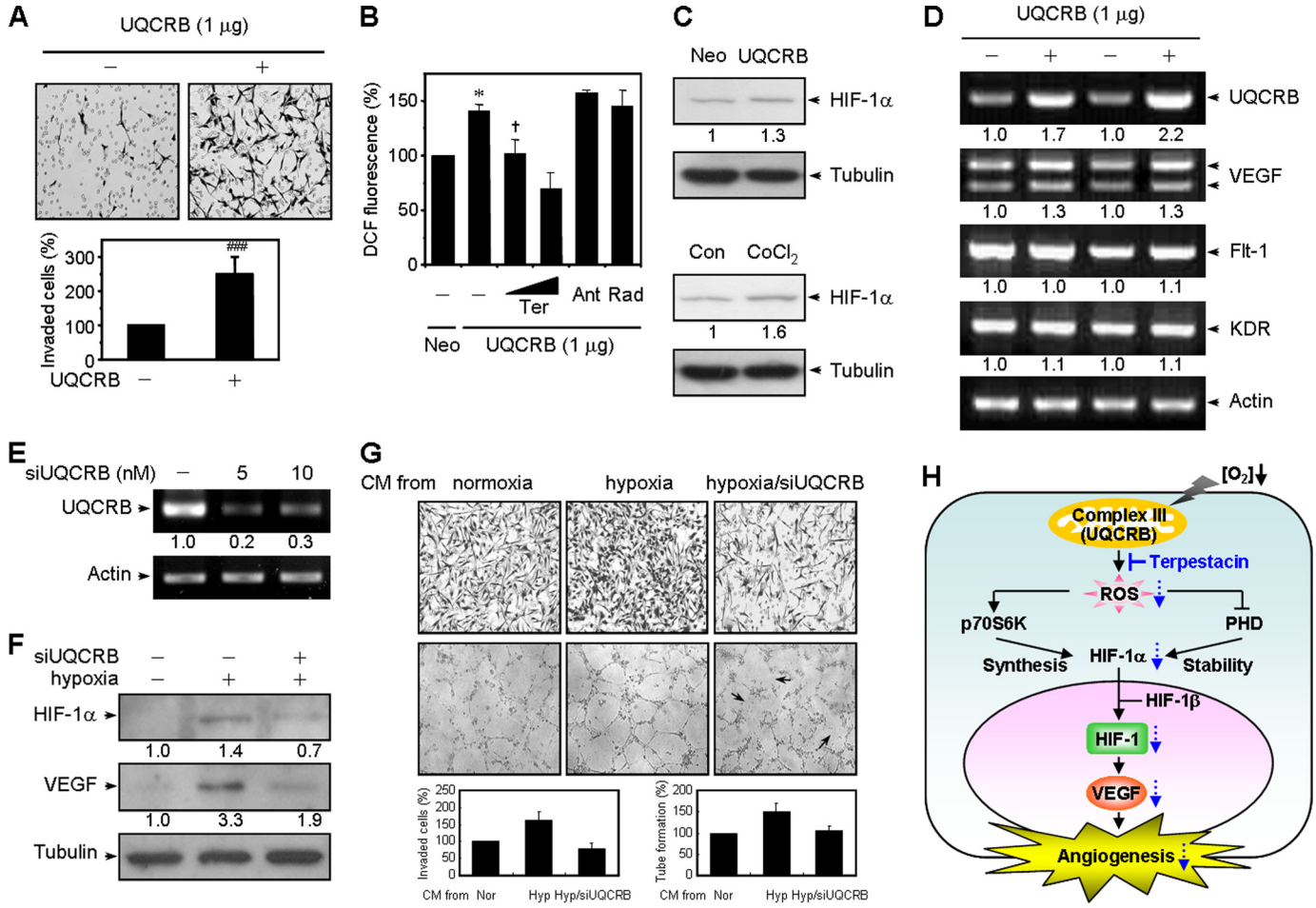

FIGURE 7. **Role of UQCRB in angiogenesis.** *A*, effect of UQCRB overexpression on tumor cell invasion. ###, $p < 0.007$ *versus* control (*Con*). The results shown are representative of three independent experiments. *B*, effect of UQCRB overexpression on mitochondrial ROS generation in HT1080 cells treated with terpestacin (20 and 40 μM), antimycin A (10 μM), or radicicol (5 μM). *, $p < 0.001$ *versus* control; †, $p < 0.006$ *versus* UQCRB overexpression. Each value represents the mean ± S.E. from three independent experiments. *DCF*, 2′,7′-dichlorofluorescein; *Neo*, control vector. *C*, effect of UQCRB overexpression on HIF-1α protein levels under normal oxygen conditions. $CoCl_2$ (100 μM) was used as a positive control. The results shown are representative of three independent experiments. *D*, effect of UQCRB overexpression on VEGF mRNA levels. The results shown are representative of three independent experiments. *E*, reverse transcription-PCR analysis shows the significant knockdown of UQCRB mRNA by siRNA. The results shown are representative of three independent experiments. *F*, effects of siRNA knockdown of UQCRB on the protein levels of HIF-1α and VEGF under hypoxia. The results shown are representative of three independent experiments. *G*, effect of UQCRB knockdown on the angiogenesis-promoting activity of HT1080 cells during hypoxia. Conditioned media (*CM*) from HT1080 cells in each culture condition were used for the endothelial cell invasion (*upper panel*) and tube formation (*lower panel*) assays. The results shown are representative of two independent experiments. *H*, the model indicates that UQCRB is a crucial component of a mitochondrial O_2 sensor in Complex III and that terpestacin binding to UQCRB inhibits the hypoxic signal transduction sequence by attenuating hypoxia-induced ROS generation, HIF-1α synthesis and stabilization, expression of VEGF, and thus tumor angiogenesis. *PHD*, prolyl hydroxylase.

the intermembrane space (28, 29) and may be involved in cellular signaling. This can be further supported by the notion that complex III-linked ROS production is mainly regulated by the redox state of the ubiquinone pool (30).

First, to investigate whether Complex III can produce ROS during hypoxia, we and other groups confirmed that myxothiazol and stigmatellin inhibit not only hypoxia-induced ROS formation but also hypoxia-induced HIF-1α stabilization (3) as shown in supplemental Fig. S3, but these small molecules do not bind to UQCRB as shown in Fig. 2*A*. Unlike the Q_o site inhibitors that prevent the formation of SQ by blocking the electron entry into Complex III and thereby blocking mitochondrial respiration and ATP generation, terpestacin suppresses hypoxia-induced ROS generation without inhibiting mitochondrial respiration, as confirmed by a mitochondrial oxygen consumption assay (Fig. 4*B*). Indeed, our present study including *in vitro* and *in vivo* experiments was performed at optimum doses of terpestacin with no cytotoxicity. Second, we also observed that terpestacin did not compete with antimycin for binding to the Q_i site of Complex III (Fig. 2*A*). Furthermore, terpestacin significantly decreased hypoxia-induced ROS production even in the presence of antimycin as shown in supplemental Fig. S4, indicating that binding of terpestacin to UQCRB might play an important role in modulating ROS production during hypoxia.

According to the three-dimensional structure of Complex III (20, 31, 32), UQCRB is a 13.4-kDa protein that resides at the bottom of cytochrome *b* where the heme b_H and Q_i site exist on the *n* side of the inner membrane (Fig. 3*A*). Our docking modeling reveals that terpestacin binds to the interface of the binding site between UQCRB and cytochrome *b*, which was confirmed through UQCRB mutagenesis studies (Fig. 3*C*). In light of this, we suggest that UQCRB may play an important role in mitochondrial ROS generation by modulating electron flux

through cytochrome *b*, thereby influencing the lifetime of the semiquinone at the Q_o site. When bound to Complex III, terpestacin seems to accelerate the forward electron transfer to the cytochrome *b*, which shortens the lifetime of SQ at the Q_o site to attenuate hypoxia-induced ROS production without blocking mitochondrial respiration. Therefore, we propose that during hypoxia, terpestacin bound to UQCRB of Complex III may mimic a condition where partially oxidized ubiquinone pool slows down the forward electron transfer to induce a reverse electron transfer onto O_2 by reduced heme b_L, resulting in the prolonged lifetime of SQ at the Q_o pocket, thereby enhancing the probability of superoxide production as was the case with antimycin-induced ROS production (23, 30). In addition, recent evidence has revealed that the membrane potential enhances the formation of superoxide from Complex III by opposing electron transfer from heme b_L to b_H (33). Indeed, the binding of terpestacin to UQCRB decreases the mitochondrial membrane potential as shown in Fig. 4*A*, suggesting that the inhibition of ROS generation by terpestacin might correlate with the lowered membrane potential. We have also confirmed that the decrease of mitochondrial membrane potential by terpestacin treatment is not associated with the disruption of the functional structure of Complex III, because terpestacin binding to UQCRB did not cause the dissociation of the subunit from Complex III (supplemental Fig. S5). Nonetheless, we still cannot exclude the possibility that terpestacin could interact directly with ROS released to the matrix or to the intermembrane space, but in either case it is clear that terpestacin renders Complx III incapable of transducing hypoxia into an ROS signal that mediates protective responses in the cell.

Terpestacin Provides a Unique Tool to Regulate Tumor Progression by Acting at the Cellular Oxygen Sensor—Our findings indicate that UQCRB performs two independent functions related to (*a*) electron transport at Complex III and (*b*) mediating cellular O_2 sensing by modulating ROS production at Complex III in response to hypoxia. UQCRB is known to play a pivotal role in the assembly and maintenance of Complex III, which is conserved in the respiratory chain of all aerobic organisms as well as in the electron transfer systems of chloroplasts and photosynthetic bacteria (34, 35). Hereditary defects in the UQCRB gene cause several mitochondrial diseases such as hypoglycemia, lactic acidosis, myopathy, and cardiomyopathy (36, 37), which are partially associated with deregulation of angiogenesis (38, 39). These diverse phenotypes may arise because various genetic mutations could differentially affect the two functions of UQCRB, namely electron transfer/bioenergetics and/or O_2-sensing functions of mitochondria. It is also noteworthy that UQCRB recently turned out to be overexpressed in 218 hepatocellular carcinoma specimens from a microarray study, implying that the gene plays a significant role in tumorigenesis (40). Accordingly, the small molecule terpestacin may serve as a unique and reversible tool for regulating UQCRB function in regard to O_2 sensing, without affecting expression levels of the protein. Furthermore, it represents a potential landmark in the development of new anti-angiogenic drugs targeting the mitochondrial O_2 sensor. Although myxothiazol and stigmatellin also block hypoxia-induced ROS signaling, the toxicity resulting from inhibition of the electron transport chain renders these and similar compounds useless as clinical tools. Conceptually, a drug that interferes with the ability of cells to detect and signal hypoxia without inhibiting respiration would be ideal as an anti-tumor agent because it would undermine the ability to activate HIF-mediated transcription in the tumor cells. In addition to mediating the angiogenesis response, HIF regulates the expression of a diverse set of genes that participate in cell proliferation, cell migration, and cell survival under conditions of hypoxic stress. These functions all contribute to tumor survival and progression, and excessive HIF activation has been correlated with poor clinical prognosis in a number of different types of cancer (41, 42). The ability of terpestacin to suppress tumor angiogenesis *in vivo* without apparent systemic toxicity underscores its potential utility, or that of its derivatives, as a new anticancer agent targeting UQCRB that plays a key role as the mitochondrial O_2 sensor.

Acknowledgments—We are grateful to Drs. Jin Han and Hiroyuki Osada for mitochondrial oxygen consumption assay, Drs. Edward Berry and Dong Woo Lee for critical and helpful discussion on the three-dimensional structural analysis of Complex III, and Drs. Hinda Kleinman, Sung-Hou Kim, and Young-Ki Paik for critical comments on the manuscript.

REFERENCES

1. Folkman, J. (1992) *Semin. Cancer Biol.* **3,** 65–71
2. Andreyev, A. Y., Kushnareva, Y. E., and Starkov, A. A. (2005) *Biochemistry* **70,** 200–214
3. Guzy, R. D., Hoyos, B., Robin, E., Chen, H., Liu, L., Mansfield, K. D., Simon, M. C., Hammerling, U., and Schumacker, P. T. (2005) *Cell Metab.* **1,** 401–408
4. Chandel, N. S., Maltepe, E., Goldwasser, E., Mathieu, C. E., Simon, M. C., and Schumacker, P. T. (1998) *Proc. Natl. Acad. Sci. U.S.A.* **95,** 11715–11720
5. Brunelle, J. K., Bell, E. L., Quesada, N. M., Vercauteren, K., Tiranti, V., Zeviani, M., Scarpulla, R. C., and Chandel, N. S. (2005) *Cell Metab.* **1,** 409–414
6. Lin, X., David, C. A., Donnelly, J. B., Michaelides, M., Chandel, N. S., Huang, X., Warrior, U., Weinberg, F., Tormos, K. V., Fesik, S. W., and Shen, Y. (2008) *Proc. Natl. Acad. Sci. U.S.A.* **105,** 174–179
7. Ulanovskaya, O. A., Janjic, J., Suzuki, M., Sabharwal, S. S., Schumacker, P. T., Kron, S. J., and Kozmin, S. A. (2008) *Nat. Chem. Biol.* **4,** 418–424
8. Kwon, H. J. (2003) *Curr. Med. Chem.* **10,** 717–736
9. Schreiber, S. L. (1998) *Bioorg. Med. Chem.* **6,** 1127–1152
10. Jung, H. J., Lee, H. B., Kim, C. J., Rho, J. R., Shin, J., and Kwon, H. J. (2003) *J. Antibiot.* (*Tokyo*) **56,** 492–496
11. Oka, M., Iimura, S., Tenmyo, O., Sawada, Y., Sugawara, M., Ohkusa, N., Yamamoto, H., Kawano, K., Hu, S. L., and Fukagawa, Y. (1993) *J. Antibiot.* (*Tokyo*) **46,** 367–373
12. Myers, A. G., Siu, M., and Ren, F. (2002) *J. Am. Chem. Soc.* **124,** 4230–4232
13. Chan, J., and Jamison, T. F. (2004) *J. Am. Chem. Soc.* **126,** 10682–10691
14. Suzuki, H., Hosokawa, Y., Toda, H., Nishikimi, M., and Ozawa, T. (1988) *Biochem. Biophys. Res. Commun.* **156,** 987–994
15. Shim, J. S., Lee, J., Park, H. J., Park, S. J., and Kwon, H. J. (2004) *Chem. Biol.* **11,** 1455–1463
16. Park, H. J., Cho, H. Y., and Kong, K. H. (2005) *J. Biochem. Mol. Biol.* **38,** 232–237
17. Shim, J. S., Lee, H. K., Park, H. M., Kim, J. O., Kim, E. K., Hwang, K. H., Kim, K. T., Park, S. W., Lee, J. H., and Kwon, H. J. (2005) *Exp. Mol. Med.* **37,** 365–370
18. Marton, M. J., DeRisi, J. L., Bennett, H. A., Iyer, V. R., Meyer, M. R., Roberts, C. J., Stoughton, R., Burchard, J., Slade, D., Dai, H., Bassett, D. E.,

Jr., Hartwell, L. H., Brown, P. O., and Friend, S. H. (1998) *Nat. Med.* **4,** 1293–1301
19. Piggott, A. M., and Karuso, P. (2008) *Chembiochem.* **9,** 524–530
20. Zhang, Z., Huang, L., Shulmeister, V. M., Chi, Y. I., Kim, K. K., Hung, L. W., Crofts, A. R., Berry, E. A., and Kim, S. H. (1998) *Nature* **392,** 677–684
21. García-Maceira, P., and Mateo, J. (2009) *Oncogene* **28,** 313–324
22. Hwang, K. Y., Oh, Y. T., Yoon, H., Lee, J., Kim, H., Choe, W., and Kang, I. (2008) *Neurosci. Lett.* **444,** 264–269
23. Berry, E. A., Guergova-Kuras, M., Huang, L. S., and Crofts, A. R. (2000) *Annu. Rev. Biochem.* **69,** 1005–1075
24. Darrouzet, E., Moser, C. C., Dutton, P. L., and Daldal, F. (2001) *Trends Biochem. Sci.* **26,** 445–451
25. Trumpower, B. L. (1990) *J. Biol. Chem.* **265,** 11409–11412
26. Guzy, R. D., and Schumacker, P. T. (2006) *Exp. Physiol.* **91,** 807–819
27. Cape, J. L., Bowman, M. K., and Kramer, D. M. (2007) *Proc. Natl. Acad. Sci. U.S.A.* **104,** 7887–7892
28. Turrens, J. F., Alexandre, A., and Lehninger, A. L. (1985) *Arch. Biochem. Biophys.* **237,** 408–414
29. Chen, Q., Vazquez, E. J., Moghaddas, S., Hoppel, C. L., and Lesnefsky, E. J. (2003) *J. Biol. Chem.* **278,** 36027–36031
30. Dröse, S., and Brandt, U. (2008) *J. Biol. Chem.* **283,** 21649–21654
31. Xia, D., Yu, C. A., Kim, H., Xia, J. Z., Kachurin, A. M., Zhang, L., Yu, L., and Deisenhofer, J. (1997) *Science* **277,** 60–66
32. Iwata, S., Lee, J. W., Okada, K., Lee, J. K., Iwata, M., Rasmussen, B., Link, T. A., Ramaswamy, S., and Jap, B. K. (1998) *Science* **281,** 64–71
33. Rottenberg, H., Covian, R., and Trumpower, B. L. (2009) *J. Biol. Chem.* **284,** 19203–19210
34. Mulder, W., Scholten, I. H., van Roon, H., and Grivell, L. A. (1994) *Biochim. Biophys. Acta* **1219,** 719–723
35. Hemrika, W., De Jong, M., Berden, J. A., and Grivell, L. A. (1994) *Eur. J. Biochem.* **220,** 569–576
36. Haut, S., Brivet, M., Touati, G., Rustin, P., Lebon, S., Garcia-Cazorla, A., Saudubray, J. M., Boutron, A., Legrand, A., and Slama, A. (2003) *Hum. Genet.* **113,** 118–122
37. Borisov, V. B. (2004) *Ital. J. Biochem.* **53,** 34–40
38. Satake, S., Kuzuya, M., Miura, H., Asai, T., Ramos, M. A., Muraguchi, M., Ohmoto, Y., and Iguchi, A. (1998) *Biol. Cell* **90,** 161–168
39. Spector, J. A., Mehrara, B. J., Greenwald, J. A., Saadeh, P. B., Steinbrech, D. S., Bouletreau, P. J., Smith, L. P., and Longaker, M. T. (2001) *Am. J. Physiol. Cell Physiol.* **280,** C72–C80
40. Jia, H. L., Ye, Q. H., Qin, L. X., Budhu, A., Forgues, M., Chen, Y., Liu, Y. K., Sun, H. C., Wang, L., Lu, H. Z., Shen, F., Tang, Z. Y., and Wang, X. W. (2007) *Clin. Cancer Res.* **13,** 1133–1139
41. Semenza, G. L. (2003) *Nat. Rev. Cancer* **3,** 721–732
42. Hong, S. S., Lee, H. S., and Kim, K. W. (2004) *Cancer Res. Treat.* **36,** 343–353